Tranverse energy and charged particle multiplicity in p-nucleus collisions at 14.6 GeV/c

J. Barrette,[3] R. Bellwied,[6] P. Braun-Munzinger,[6] W.E. Cleland,[5] T. Cormier,[8] G. David,[6] J. Dee,[6] G.E. Diebold,[9] O. Dietzsch,[7] J.V. Germani,[9] S. Gilbert,[3] S.V. Greene,[9] J.R. Hall,[4] T.K. Hemmick,[9] N. Herrmann,[6] B. Hong,[6] K. Jayananda,[5] D. Kraus,[5] B.S. Kumar,[9] R. Lacasse,[3] D. Lissauer,[1] W.J. Llope,[6] T. Ludlam,[1] R. Majka,[9] S.K. Mark,[3] J.T. Mitchell,[9] M. Muthuswamy,[6] E. O'Brien,[1] C. Pruneau,[3] M. Rosati,[3] F.S. Rotondo,[9] N.C. da Silva,[7] U. Sonnadara,[5] J. Stachel,[6] H. Takai,[1] E.M. Takagui,[5] G. Wang,[3] C.L. Woody,[1] N. Xu,[6] Y. Zhang,[6] Z. Zhang,[5] and C. Zou[6]

(E814 Collaboration)

[1]*Brookhaven National Laboratory, Upton, New York 11973*
[2]*Los Alamos National Laboratory, Los Alamos, New Mexico 87545*
[3]*McGill University, Montreal, Quebec, Canada H3A 2B2*
[4]*University of New Mexico, Albuquerque, New Mexico 87131*
[5]*University of Pittsburgh, Pittsburgh, Pennsylvania 15260*
[6]*State University of New York, Stony Brook, New York 11794*
[7]*Universidade de São Paulo, São Paulo, Brazil*
[8]*Texas A&M University, College Station, Texas 77843*
[9]*Yale University, New Haven, Connecticut 06511*

(Received 23 January 1995)

We present the transverse energy distributions, $d\sigma/dE_T$ and $dE_T/d\eta$, and the charged particle multiplicity distributions, $d\sigma/dN_c$ and $dN_c/d\eta$, produced in p+Al and p+Pb collisions at 14.6 GeV/c. The data exhibit a weak correlation between these global variables. While a significant increase of the mean multiplicity with the mass of the target is observed, the transverse energy distributions show little target dependence. The $dE_T/d\eta$ distribution shifts backward as the mass of the target increases, indicating the presence of rescattering. The data are compared to the predictions of the relativistic quantum molecular dynamic model (RQMD) and Fritiof event generators. RQMD reproduces well the main features of the data while Fritiof predicts too forward peaked transverse energy and particle multiplicity pseudorapidity distributions.

PACS number(s): 25.75.+r, 13.85.−t

I. INTRODUCTION

In the last few years, studies of heavy-ion reactions at high energy have provided new insight into the production of nuclear matter at high baryon density and temperature. The main goal of this research is to evidence and study the expected new phase of nuclear matter that would result from the deconfinement of the quarks and gluons. To understand the signatures resulting from the production of this new form of nuclear matter (or any new phenomenon) and to succeed in deducing its properties, it is important that we have a quantitative understanding of the heavy-ion reaction mechanisms in all kinematic regions that are present in the collisions.

It has been shown that at alternating-gradient synchroton (AGS) energies (10–15 GeV/nucleon) full stopping is achieved in Si+Pb reactions [1,2]. The exponential behavior of the invariant cross section of the produced particles as a function of the transverse momentum (or transverse mass m_T) [3] and the delta resonance population [4] indicate that some degree of thermal equilibrium has been reached. However, the rapidity dependence of the particle distribution [2,5] and the variation of the slope constant of the p_T spectra with the mass of the particles [3,6] indicate that large collective transverse and longitudinal expansions are present [7,8]. Furthermore, the large E_T values observed at backward angles in asymmetric collisions like Si+Pb and the evolution of the particle rapidity distributions with centrality indicate a large degree of rescattering at AGS energies.

While many aspects of heavy-ion collisions at AGS energies are now well characterized, it is important to study the underlying processes to clarify and test our understanding of the reaction mechanisms of these collisions. The study of $p+A$ collisions should be particularly useful to understand in which way $A+A$ collisions differ from simple superpositions of nucleon-nucleon collisions. A systematic set of measurements of the global transverse energy distributions for proton-, ^{16}O-, and ^{28}Si-induced collisions at 14.6A GeV/c has been published [9]. In this work, the transverse energy produced with heavy beams has been shown to be consistent with an incoherent superposition of contributions from $p+A$ reactions. This contrasts with the measured relative yield of the produced particles, which shows a strong variation from p+Be to p+Au, to central Si+Au collisions [10].

Many dynamic models have been proposed to describe heavy-ion collisions in this energy range [11–14]. They are similar in their implementation of the collision process as a superposition or a successive cascade of hadron-hadron collisions. The study of $p+A$ collisions may serve as a test of the validity of these models in describing the transition from a single-particle collision problem to a thermodynamic problem mainly defined by a few observables.

In heavy-ion collisions, global observables, such as the transverse energy or particle multiplicity distribution, have

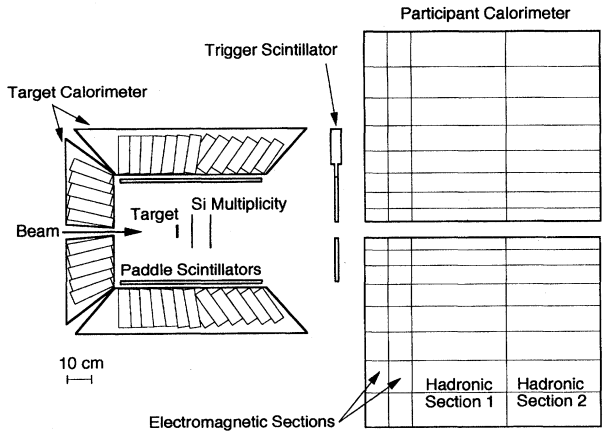

FIG. 1. Schematic diagram of the part of the E814 experimental setup used for the measurements reported in this paper.

been shown to be good indicators of the impact parameter or centrality of the collision. Furthermore, they also provide valuable information on the collision dynamics. For example, $dE_T/d\eta$ is predicted to be related to the thermal energy density, though in a model-dependent manner [15]. In this paper we report on measurements of the transverse energy and charged particle multiplicity distributions produced in proton-induced collisions on Al and Pb targets at 14.6 GeV/c. The correlation between these two global observables is discussed, and the produced tranverse energy per observed charged particle is also presented. The data are compared to the predictions of the relativistic quantum molecular dynamic (RQMD) [13] and Fritiof [12] event generators. These data were obtained using the E814 apparatus and are thus immediately comparable to data obtained for ^{28}Si-induced reactions at the same energy per nucleon [1,16,17].

The experimental setup is described briefly in the next section. The data analysis methods are considered in Sec. III. The data are presented and discussed in Sec. IV, where they are compared to the predictions of two event generators. A short summary and conclusions are given in Sec. V.

II. EXPERIMENTAL SETUP

The E814 apparatus consists mainly of two calorimeters providing nearly 4π calorimetric coverage, a charged-particle multiplicity detector, and a forward magnetic spectrometer centered at 0°. The part of the apparatus used for the measurements described here is shown in Fig. 1. More details on some of the detectors can be found in Refs. [2,16,18,19].

The experiment used a secondary proton beam produced by the Brookhaven National Laboratory (BNL) AGS accelerator complex. The momentum of the beam was on average 14.6 GeV/c with a width σ_p=0.85 GeV/c determined by the acceptance of the beam line. Valid beam particles were defined by a beam telescope installed upstream of the target. This telescope is comprised of two circular scintillator detectors of 1.3 mm and 2.5 mm thickness and of 7 mm and 15 mm diameter, respectively. They were installed 1.9 m and 6.5 m in front of the target. The size of these detectors defined the dimension and maximum divergence of the accepted beam. Thick scintillators located near each of the beam scintillators were used to veto beam particles accompanied by particles arriving outside the desired acceptance. Two multiple-strip silicon detectors installed 2.58 and 5.63 meters in front of the target were used to determine the position and direction in the horizontal plane of the incident particles at the target with a precision of about 0.07 mm and 0.012 mrad, respectively. The beam definition counters were complemented by a 2.2 m long threshold gas Cerenkov counter located in between the two Si detectors. This counter was operated with Freon at atmospheric pressure and was used to veto light particles (pions, muons, and electrons) in the secondary beam.

Energy flow was measured with two calorimeters. The forward calorimeter (PCAL) covering the pseudorapidity range $1.0 < \eta < 4.0$ is a Pb-scintillator sampling calorimeter. It is meant mainly to measure collision participants in heavy-ion collisions. It is made of four identical quadrants, each subdivided into four azimuthal sections of 22.5°, further subdivided radially into eight towers. Each tower is comprised of two electomagnetic depth segments of 0.4 interaction length each and two hadronic depth segments of 1.6 interaction length, yielding a total of 4 interaction lengths for the entire calorimeter. The light from each of the scintillators making up a tower is brought to a photomultiplier tube via wavelenght shifting optical fibers. For more details on this detector see Refs. [19,20].

The PCAL coverage is complemented at backward angles with a NaI calorimeter (TCAL) referred to as target calorimeter, since it mainly detects target fragments. This calorimeter consists of 992 NaI crystals 4 × 4 cm in cross section and 6 radiation lengths thick, arranged in four side walls and one back wall surrounding the target. The side walls cover a range, on average, of $48° < \theta_{\rm lab} < 118°$ corresponding to a pseudorapidity coverage of $-0.5 < \eta < 0.8$, while the back wall covers the range $-2.0 < \eta < -0.9$. Each NaI crystal is read out with a vacuum photodiode.

The charged-particle multiplicity is measured using two silicon pad detectors. They were made of circular silicon wafers 300 μm thick and approximately 38 mm in radius with a hole in the center for the beam. The active surface of each Si disk is divided into 512 pads arranged in concentric rings. The detectors cover the pseudorapidity interval $0.875 < \eta < 3.86$ in 20 steps. For more details concerning these detectors see Refs. [16,21].

For this experiment an additional detector (TRIG) (not part of the standard setup) was added to provide a minimum bias trigger. This detector, installed 65 cm downstream of the target, was made of a 1 cm thick disk-shaped scintillator with an outer diameter of 40 cm and a circular hole of 3.5 cm diameter in the center for the beam. It covers an angular range $3° < \theta_{\rm lab} < 17°$ and has an efficiency close to 100% for the detection of minimum ionizing particles.

Two different interaction triggers were used in the measurements of the data reported in the present paper. In a first set of measurements, the trigger was formed by requiring at least one minimum ionizing particle in the TRIG detector, and more than two particles in the multiplicity detector (*multiplicity trigger*). A trigger formed by a logical AND condi-

tion between these two detectors considerably reduces the number of false triggers due to noise in the multiplicity detector or due to stray particles hitting the TRIG detector. The interaction trigger was required for all events. The multiplicity trigger cross section was 1380 mb for the Pb target and 320 mb for Al. Additional trigger requirements were imposed at the first and second level, and events satisfying these criteria could be independently downscaled to optimize the distribution of events recorded on tape, in particular to increase the fraction of low cross-section events. The other interaction trigger used (*E_T trigger*) was defined by requiring a minimum tranverse energy of $\approx$ 1 GeV in the participant calorimeter. For trigger purposes, an estimate of PCAL tranverse energy was derived from analog sums of the signals where each phototube signal is given a weight corresponding to the sine of the angle with respect to the beam direction of the respective detector element. Simultaneously, three second level triggers were also defined corresponding to different thresholds in the PCAL transverse energy. In each run, additional triggers were generated either at random or by beam particles for the purpose of estimating background, efficiencies, noise, and pedestals.

Typical total beam intensities varied between 5×10^4 and 1.5×10^5 particles per 1 sec AGS spill. Roughly 10% of these particles met the cuts imposed by the beam definition detectors and were considered to be good beam particles. Targets of natural Al and Pb with thicknesses of 1.3 and 2.6 g/cm^2 (for Al) and 2.2 and 4.4 g/cm^2 (for Pb) were used. These thicknesses correspond to $\approx$ 1.2% and 2.4% of a nuclear interaction length for protons.

III. DATA ANALYSIS

In this section, we discuss the methods of calibration and corrections and some of the cuts and selection criteria used in the analysis of the data from the various detectors.

A combination of three cuts was used to ensure that a single proton was incident on the target close to the beam axis. These were provided by the beam scintillator telescope, the vertex detector and the back wall of the target calorimeter.

For a good beam particle, a valid signal in the two beam scintillators and the absence of signal in the external veto counters of the beam telescope was required. This condition defines the width and divergence of the beam at the target to be ±2.4 mm and ±0.9 mrad, respectively.

The vertex detector is used to determine the position and incidence angle of each beam particle at the target. Due to the close geometry of the multiplicity detector, the measured distribution of charged particles, $dN_c/d\eta$, is somewhat sensitive to the vertex position. Thus, for the multiplicity measurements described below, the vertex detector was used to determine the position of the beam particles relative to the vertical symmetry axis of the multiplicity detectors. Particles having horizontal position within ±1 mm of this axis were selected ($\approx$40% of the accepted beam particles). The center of the detector was determined by requiring that the azimuthal multiplicity distribution be isotropic when averaged over many events.

The upstream wall of the TCAL is used to veto interactions occuring upstream of the target, in the beam pipe, beam exit window, vertex detector, or beam telescope scintillators. Such events tend to deposit a much larger fraction of the detected energy in this wall than interactions occuring in the target. This veto is particularly useful with heavy-ion beams, which have larger interaction cross sections. For the data discussed here, the fraction of events rejected by this criterion amounts to ≈3 % of the interaction triggers.

The multiplicity detector is operated as a hit detector. The presence of a signal above a threshold corresponding to approximately one-half of the energy loss (most probable) of a minimum ionizing particle at normal incidence on the detector is required to register the occurrence of a charged particle in a given pad. The response of the detector is affected by the number of noisy and dead pads and the possible charge sharing between adjacent pads. The noisy and dead pads were easily identified from the analysis of normal events and those given by random triggers. Other pads have also been omitted from the analysis on the basis that their average occupancy deviates by more than two standard deviations from the average occupancy of the other pads in the same ring. As a result, roughly 5% of the pads were not included in the final analysis. This known detector inefficiency was corrected in the data presented below. From the pad to pad fluctuations in the measured multiplicity, it is estimated that the systematic error in the $dN_c/d\eta$ distributions is of the order of 5%.

The effect of charge sharing between neighboring pads for particles going through the detector close to pad boundaries has been shown to be very small [16,21] and has not been corrected for. Effects of fluctuations on the energy loss resulting in the misidentification of hits due to low energy loss are estimated to be less than 1% and have not been corrected for.

The effects of multiple hits, charge collection fluctuations, and δ rays are also estimated to be small. The multiplicity detector was designed for the study of Si-nucleus collisions. For p-nucleus collisions the average occupancy is very small. The resulting corrections for multiple hits are estimated to amount to ≈0.4 particles at multiplicity $N_c=20$ and even less at lower multiplicity. The measured multiplicity distribution of events corresponding to random triggers peaks at $N_c=0$ and has a mean value of 0.04, showing that random hits due to charge collection fluctuations are negligible. Finally, scaling from the δ-ray distributions measured with ^{28}Si beam [16], δ rays are evaluated to contribute on average less than 0.3 particles to the measured multiplicity for events with multiplicity $N_c=20$. The influence of the conversion in the target of photons originating from π^0 decay has been evaluated using the GEANT package [22] and different event generators. The results are discussed in Sec. IV below.

The energy calibration of the target calorimeter was done with cosmic-ray muons detected during two long calibration runs performed prior to and after the proton runs. Gains were typically found to vary by less than 1% between the calibration runs. Other detailed gain stability studies have shown [23] that gain fluctuations are at the 1% level and thus negligible. The pedestal levels of the ADC's were found to vary over extended periods of time. They have been monitored and adjusted off line run by run using random trigger events. The pedestal width of individual channels is typically 1 MeV, while the pedestal width of the energy sum of all channels is

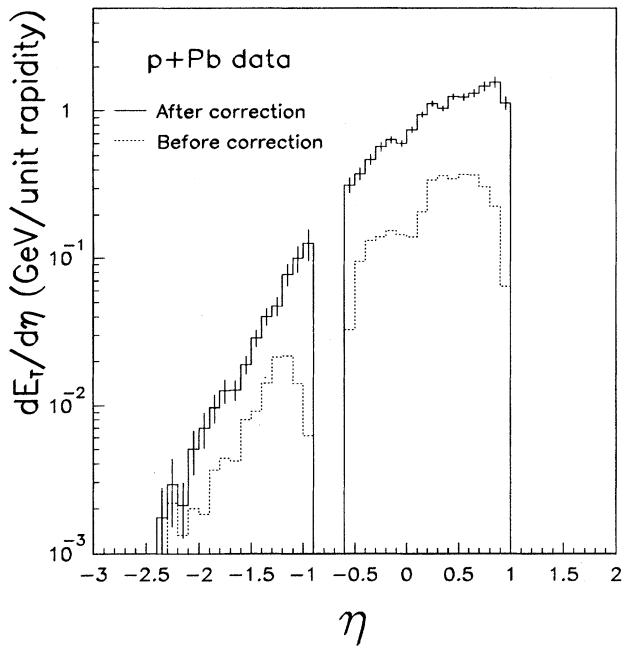

FIG. 2. Experimental $dE_T/d\eta$ distributions as measured by the TCAL for the Pb target before corrections for leakage (dotted histogram) and after corrections are applied (solid histogram).

typically 150 MeV, indicating the presence of some coherent noise. A cluster search algorithm was used to determine the total-energy deposition in the TCAL and to minimize coherent noise effects. In this algorithm, a local maximum is first searched for. If its energy exceeds 2.5 MeV, it is considered as defining a cluster center, and the energy of the neighboring crystals is summed to get the cluster energy. The crystals that do not belong to any cluster are not considered.

The leakage and geometrical corrections were estimated by tracking, using GEANT, particles from events generated using various models. The effect of this correction is shown in Fig. 2, where we present the experimental $dE_T/d\eta$ distribution for the p+Pb reaction. The dashed lines correspond to the measured energy before corrections for the response of the target calorimeter. Most of the structure in these distributions is due to the granularity and acceptance of the target calorimeter. The corrected data obtained using correction factors deduced from the RQMD model are shown by the solid histogram. In order to evaluate the reliability of the corrections, correction factors were also obtained by tracking events generated using the HIJET [11,24] and Lund-Fritiof [12] models, which produce different particle distributions. The η dependence of the correction factors is very similar for all models. The main difference is in the overall scale of the correction, which varies by up to 10% from one model to the other.

The response of the participant calorimeter to particles of energy ranging from 0.25 to 7 GeV has been studied in detail [20,25]. The measured energy resolution for electrons varies from $0.24/\sqrt{E(\mathrm{GeV})}$ to $0.32/\sqrt{E(\mathrm{GeV})}$ depending on the tower. The hadronic resolution after correction for transverse and longitudinal leakage is $\approx 0.4/\sqrt{E(\mathrm{GeV})}$ for particle kinetic energies above 0.25 GeV.

The PCAL has two monitoring systems. An optical source system is used to set and monitor the photomultiplier tube gains. In addition, a ^{60}Co source system is used to determine the long-term stability and the relative plate-to-plate response of the calorimeter. A number of tests have been performed to study the reproducibility and stability of the gain settings. Gain shifts smaller than 3% have been observed over periods of time comparable with the data taking period. These small gain variations have not been corrected for. Pedestals shifts were monitored and, as with the TCAL, adjusted run by run.

As discussed in Refs. [19,20], the calorimeter responds rather differently to various types of particles. Futhermore, as shown in Fig. 1, this detector does not have a projective geometry towards the target. This leads to a nontrivial relation between the incident energy distribution and the energy deposited in the different towers. To obtain corrected $dE_T/d\eta$ distributions, we employ a response-matrix approach, which is described in more detail in Ref. [26]. Advantages of this method are that it takes into account the leakage between different angular intervals due to shower spread and incorporates the longitudinal shower profile information into the correction. In the present analysis, the incoming energy flow is binned into eight intervals in pseudorapidity according to the radial granularity of the calorimeter. The response matrix was calculated using simulated events for p+A collisions from the RQMD event generator. We have estimated the systematic errors associated with this method by applying it to tracked events from various event generators (RQMD, Fritiof, and HIJET [11]). The systematic error is estimated to be less than 10% for all bins except at the largest angle ($\eta \approx 0.9$) where, because of energy leakage, the error is $\approx$ 15%.

IV. RESULTS AND DISCUSSION

The differential cross sections for E_T production measured in the participant and the target calorimeter are shown in Figs. 3 and 4, respectively, for the Al and Pb targets. The data of Fig. 3 were obtained using the E_T *trigger*. This explains the observed fall off at low E_T. The data in Fig. 4 were obtained with the *multiplicity trigger*. These data are not corrected for leakage. The larger cross section for Pb is mainly due to the larger reaction cross section of heavier target nuclei. The shape of the E_T distributions measured with the participant calorimeter is almost identical for the two targets, while in the solid angle covered by the target calorimeter one observes a strong increase of E_T for the heavier target.

These results are compared to the predictions of the RQMD and Lund-Fritiof models. The calculations take into account the effect of trigger bias and detector leakage. However, the trigger bias has relatively little effect on the overall shape of the E_T distributions above the trigger threshold. Both models produce very similar results in the participant calorimeter acceptance. They describe fairly well the shape of the E_T distributions but slightly underestimate the average value of the produced E_T. These event generators, however, give very different results in the backward region covered by the target calorimeter. While RQMD describes the experimental data very well, Fritiof strongly underestimates the

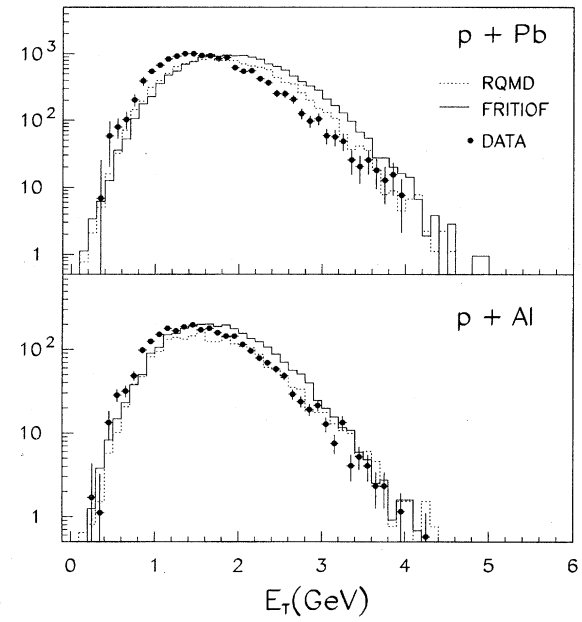

FIG. 3. Experimental transverse energy spectra as measured by the PCAL for the $p+$Pb (top) and $p+$Al (bottom) reactions. The histograms are the predictions of the RQMD (dotted lines) and Fritiof (solid lines) model. The error bars represent the statistical errors.

production of transverse energy for both targets.

Some insight on the origin of this behavior is obtained from the rapidity dependence of the E_T distributions shown in Fig. 5. These data have been corrected to take into account

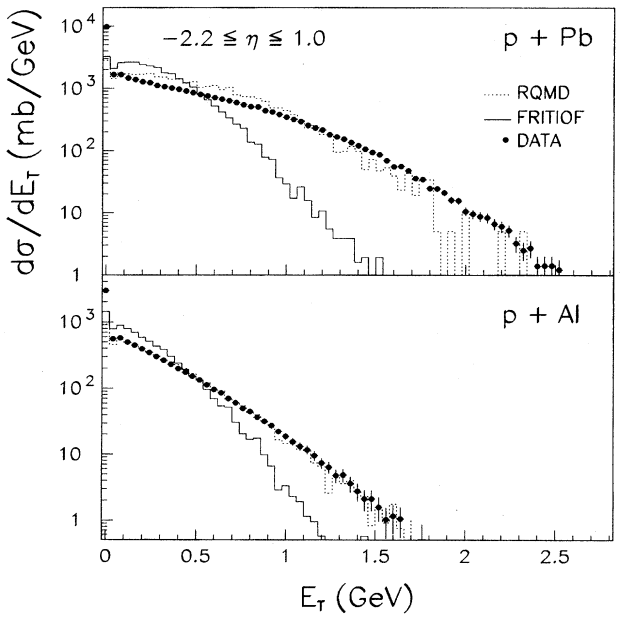

FIG. 4. Experimental transverse energy spectra as measured by the TCAL for the $p+$Pb (top) and $p+$Al (bottom) reactions. The data are not corrected for energy leakage. The error bars represent the statistical errors.

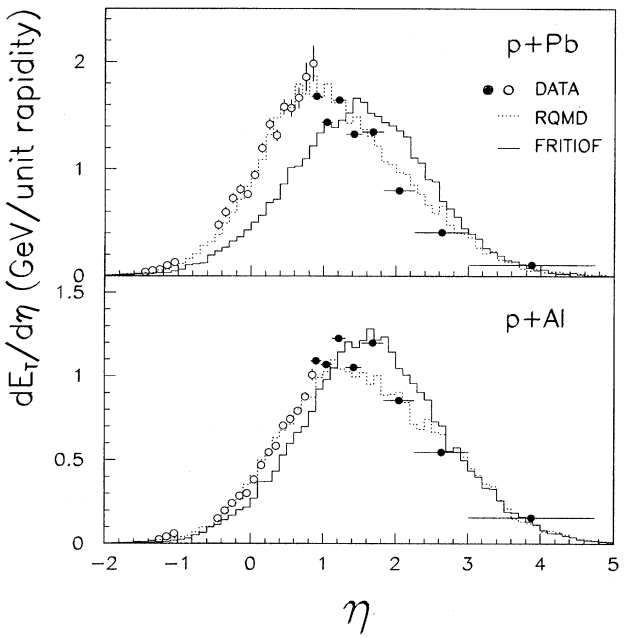

FIG. 5. Corrected $dE_T/d\eta$ distribution for $p+$Pb (top) and $p+$Al (bottom) reactions. The open dots are obtained with the TCAL, while the closed dots are obtained with the PCAL. The histograms are the results of model calculations: RQMD (dotted lines) and Fritiof (solid lines).

leakage and the response of the detector following the methods described in the preceding section. Both experimental distributions are roughly Gaussian in shape with a width $\sigma_\eta \approx 0.9$ units of pseudorapidity. The $p+$Pb distribution, however, peaks at a lower pseudorapidity. This shift can be considered a measure of the importance of secondary interactions in the collision. RQMD describes very well the experimental distributions including their evolution with target mass. Fritiof reproduces the measured integrated transverse energy, but it results in a systematically too small rapidity shift. The effect is particularly striking for the $p+$Pb reaction. In fact, this model predicts, for both targets, distributions that peak close to the nucleon-nucleon center-of-mass rapidity ($\eta=1.7$). The good description provided by RQMD persists even in the tail of the E_T distributions, as shown in Fig. 6.

The measured charged particle multiplicity distributions, $d\sigma/dN_c$, obtained with the multiplicity trigger are shown in Fig. 7. Note that the data point at $N_c=1$ has probably an important contribution from noninteracting beam particles. As expected, one observes a sizable increase in multiplicity for the heavier Pb target with multiplicities reaching more than 30 for the most inelastic collisions. For the Al target the distribution peaks below the trigger cutoff, while for Pb, the multiplicity distribution peaks at $N_c \approx 7$. At high multiplicity the cross section decreases exponentially with multiplicity for both targets. This target dependence is relatively well reproduced by RQMD. However, this model predicts a sharper decrease at high multiplicity than is observed. Fritiof produces very similar results. In the simulations only protons with kinetic energy larger than 60 MeV have been included so as to reject particles that in the models come from the

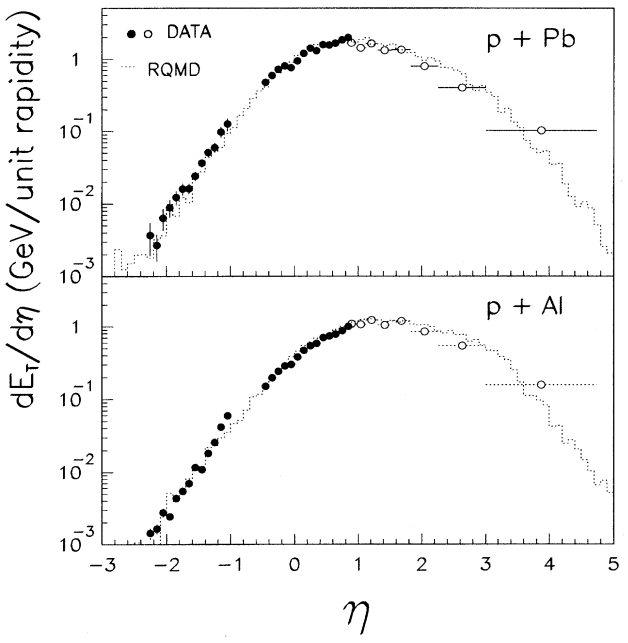

FIG. 6. Corrected $dE_T/d\eta$ distribution for p+Pb (top) and p+Al (bottom) reactions plotted on a semilogarithmic scale to enhance the results in the tail of the distributions at low pseudorapidity.

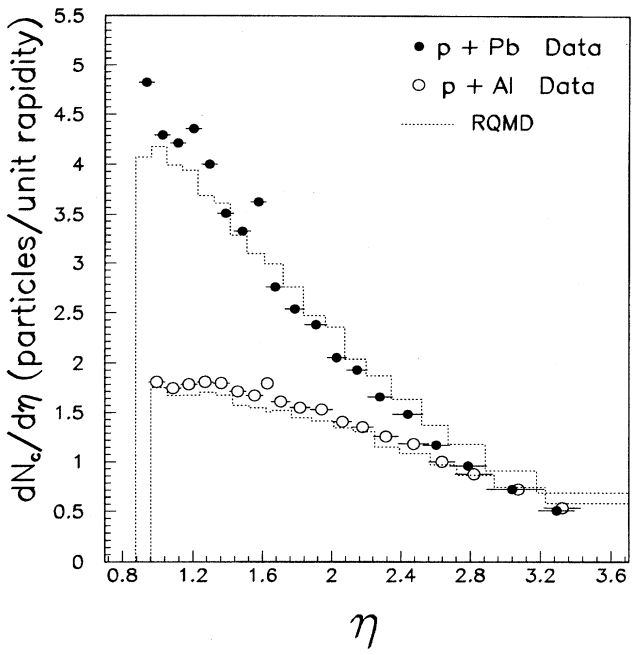

FIG. 8. Pseudorapidity distributions of charged particle multiplicity for p+Pb (full dots) and p+Al (open dots) reactions. The histograms are predictions of event generators: RQMD (dotted lines).

dissociation of the unbound target with energies characteristic of the Fermi energy. The effect of particle interaction and photon conversion in the target has been included. For the Pb target, photon conversion is calculated to add, on average, one particle to the measured multiplicity. For the Al target the effect is negligible. The multiplicity detector has a very low threshold and is sensitive to charged particles of all energies including low-energy target fragments and evaporated particles. This could explain in part the observed discrepancy at high multiplicity. Note that once taken into account, the trigger bias at low multiplicity RQMD gives total cross sections (1386 mb for Pb and 272 mb for Al) that reproduce fairly well the experimental multiplicity trigger cross sections.

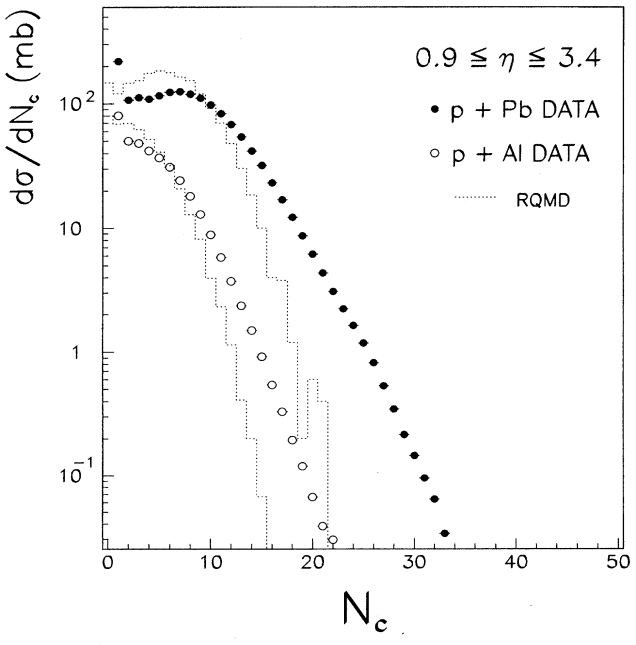

FIG. 7. Comparison of the measured charged-particle multiplicity distribution $d\sigma/dN_c$ for p+Pb and p+Al reactions with the predictions of RQMD (dotted lines).

An important and interesting target dependence is observed in the pseudorapidity distribution of the charged particles, $dN_c/d\eta$, presented in Fig. 8. The additional multiplicity for the Pb target is centered at low pseudorapidity in the target region, while the charged particle multiplicity is independent of the mass of the target near beam rapidity. This shows that near beam rapidity the multiplicity is determined by the first p-nucleon collision, while at backward angles secondary interactions lead to larger multiplicities for larger targets. This dependence is perfectly well reproduced by RQMD. On the other hand, as for the transverse energy (Fig. 5), version 1.7 of Fritiof, which does not include rescattering of secondaries, produces a peak at half the beam rapidity and fails completely to reproduce the data.

The evolution of the pseudorapidity distribution of charged particles as a function of the total multiplicity is shown in Fig. 9 for the Pb target. It is interesting to note that the distributions converge at high pseudorapidity and are equal within error at beam rapidity. As the total multiplicity increases the additional multiplicity appears mainly at the lowest pseudorapidity in the target region, a behavior similar to that observed in Fig. 8. In the bottom part of the figure we

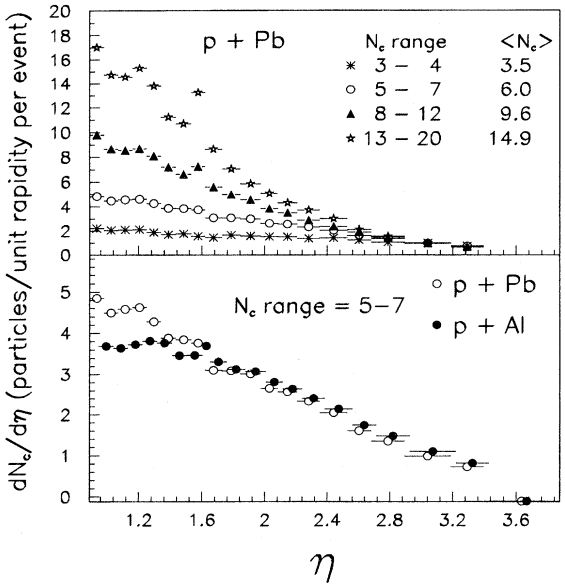

FIG. 9. Upper frame: Pseudorapidity distributions of charged particle multiplicity $dN_c/d\eta$ for $p+$Pb reaction for various cuts in the total multiplicity. Lower frame: Comparison of the pseudorapidity distribution of the particle multiplicity for $p+$Pb and $p+$Al for a similar cut in the total multiplicity.

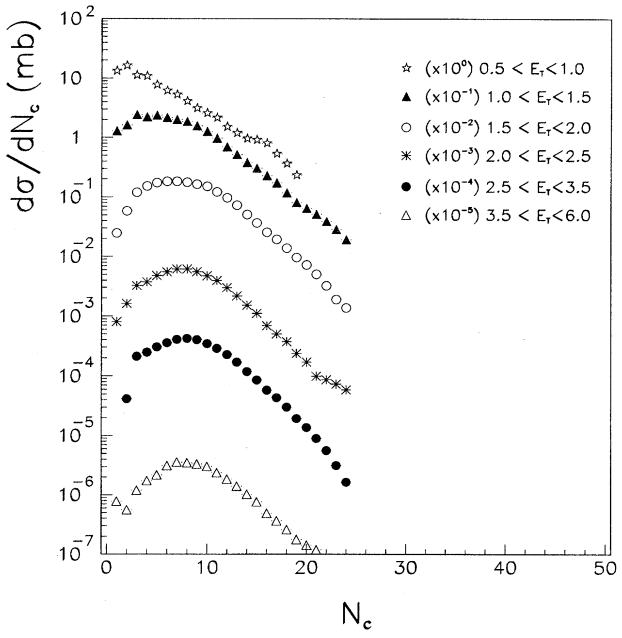

FIG. 10. Charged-particle multiplicity distributions for various cuts in the transverse energy measured in the PCAL for the Pb target.

compare the pseudorapidity distribution for Al and Pb targets for equivalent total multiplicity. These distributions have very similar shapes with the only difference appearing at pseudorapidity < 1.4. A very similar behavior is observed for the other slices in total multiplicity.

With heavy projectiles, a very strong correlation is observed between the produced transverse energy and the charged-particle multiplicity. In the case of $p+A$ collisions this correlation is much weaker. This is shown in Fig. 10 where the multiplicity distributions for various cuts in the transverse energy measured in the PCAL (see Fig. 3) are presented for the $p+$Pb reaction. Except for the distribution corresponding to the lowest energy detected in the PCAL, where the multiplicity peaks at the trigger threshold of the multiplicity detector, all distributions are very similar and show little dependence on the measured transverse energy. This behavior is better quantified in Fig. 11 where the evolution of the mean value and the variance of the multiplicity distribution as a function of the transverse energy are presented. The width of the distribution is, within the experimental error, independent of the transverse energy and is, over most of the E_T range, much larger than the shift in the observed mean multiplicity. The experimental behavior is quite well reproduced by the RQMD calculations. However, the calculations predict slightly narrower distributions and a stronger correlation between E_T and N_c.

Figure 12 shows the η distribution of transverse energy produced per charged particle in the overlapping acceptance of the PCAL and multiplicity detector. It is obtained from the ratio between the data of Fig. 5 and Fig. 8, respectively. For this figure, the $dN_c/d\eta$ data have been rebinned according to the coarser binning of the PCAL data. The distributions are relatively flat with a weak maximum near the nucleon-nucleon center of mass rapidity ($\eta=1.7$). A somewhat larger value is observed for the Al target indicating that the available energy is divided over fewer nucleons of the target. This trend is well reproduced by both models. The η dependence

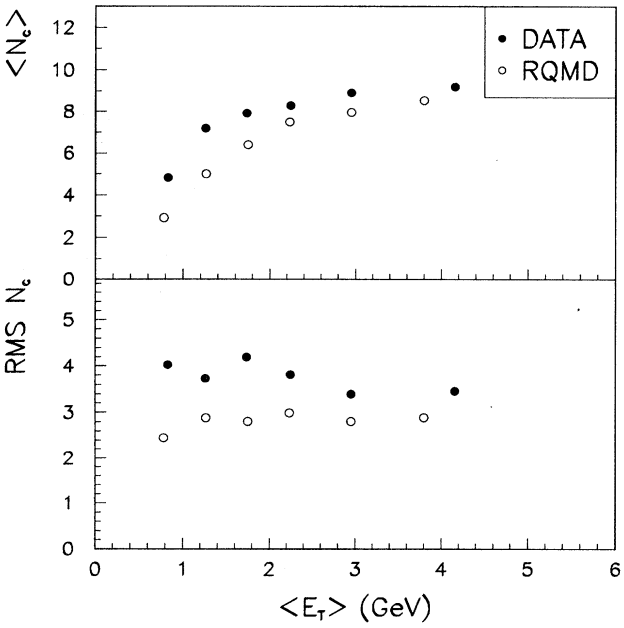

FIG. 11. Comparison of the mean value (top) and variance (bottom) of the charged particle multiplicity distributions as a function of the transverse energy in the PCAL for the Pb target (full dots) with the results from RQMD (open dots).

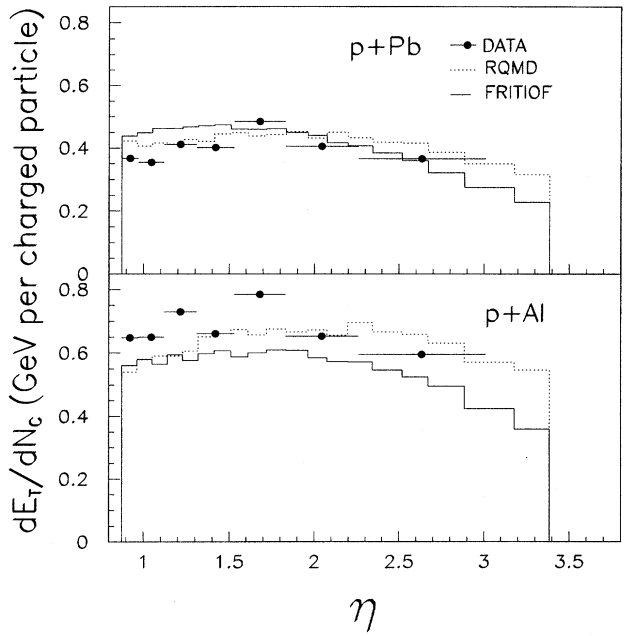

FIG. 12. Transverse energy per charged particle for $p+$Pb (top) and $p+$Al (bottom) in the pseudorapidity acceptance of the PCAL. The histograms are predictions of various event generators.

over this pseudorapidity range is also well predicted by both models, in spite of the fact that Fritiof fails in describing both the E_T and charged-particle pseudorapidity distributions. This indicates that a good description of the E_T per particle can be somewhat fortuitous.

In Fig. 13, we present the η distribution of E_T per cluster of energy in the target calorimeter (see Sec. III for definition of cluster). To generate this figure the corrected E_T values shown in Fig. 5 are used. The number of energy clusters in TCAL is strongly correlated with the number of produced particles. However, these results cannot be directly compared to those of Fig. 12, since the efficiency of the TCAL varies considerably with particle type. There is roughly a 10% probability that a neutron emitted in the η acceptance of the TCAL produces a cluster, while a π^0 on average produces more than one cluster because of the TCAL sensitivity to photons. The mean number of clusters is 2.7 and 7.5 for the Al and Pb targets, respectively, and on average a cluster includes three crystals of the TCAL. The nearly flat distribution observed over the PCAL acceptance persists down to $\eta \approx 0$, and then the energy per cluster decreases as we move to backward angles. As at forward angles, the absolute value and shape of the distributions are very well reproduced by RQMD. To generate the calculated distributions, the generated particles were tracked through the TCAL using GEANT, and the cluster algorithm was applied to the calculated energy deposition in the TCAL crystals.

In Fig. 14 we compare the pseudorapidity distribution of E_T per charged particle for $p+$Pb and Si+Pb reactions at the same bombarding energy per nucleon. The data for Si+Pb are taken from Refs. [16,27] and correspond to the 7% most central collisions. The distributions are relatively flat but there is an indication of a shift of the maximum towards lower pseudorapidity for the Si+Pb system. On average, the energies for Si+Pb are 10–20 % larger than for the $p+$Pb reaction. This is consistent with the increase in the average p_T of the proton spectra between $p+$Au and Si+Au reac-

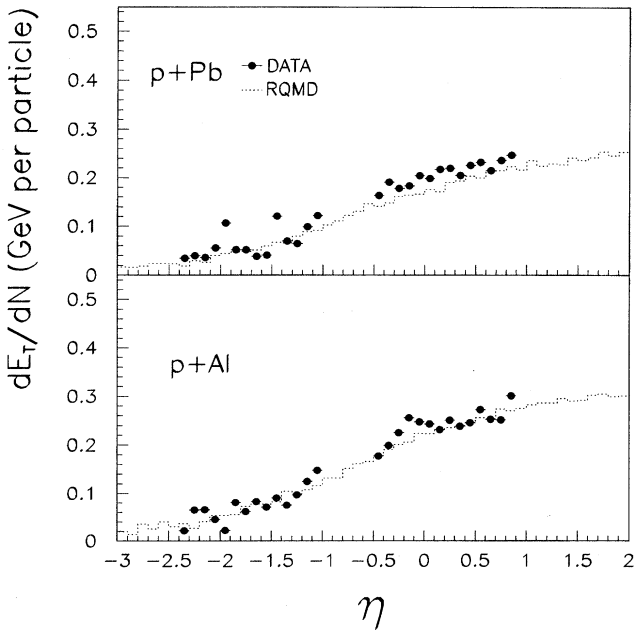

FIG. 13. Pseudorapidity distribution of the mean transverse energy per cluster observed in the TCAL. The histograms are the predictions of the RQMD event generator.

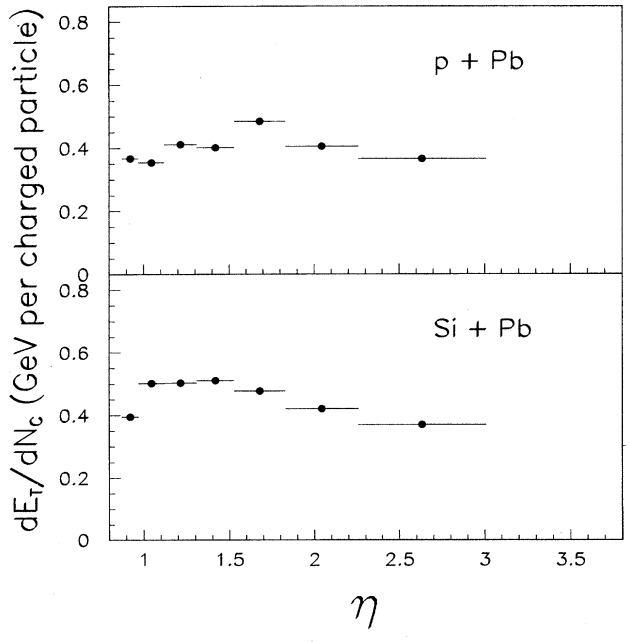

FIG. 14. Transverse energy per particle for the $p+$Pb (top) and Si+Pb (bottom) reactions. The data for Si+Pb are obtained from Refs. [14,25] and are for the 7% most central collisions. The $p+$Pb data are from a minimum bias trigger.

tions at the same energy reported in Ref. [28] and with the measured increase of the inverse slope parameters of the particle spectra for the same reactions [29].

V. CONCLUSIONS

In this paper, we have presented extensive measurements of the transverse energy and charged-particle multiplicity distributions produced by proton-induced reactions on Al and Pb targets at 14.6 GeV/c. The evolution of the measured global observables with the mass of the target reinforces the conclusion, based on measurements with heavier beams, that significant rescattering or multiple scattering is present and contributes to the evolution of the energy deposition in the colliding system. This must be taken into account in the models used to describe heavy-ion collisions, since rescattering of the secondaries strongly influences the space-time evolution of the energy density distribution in heavy-ion reaction and thus is relevant to the maximum energy density reached in such collisions.

The RQMD event generator reproduces very well all the features of the data, giving confidence that this model provides a good representation of heavy-ion collisions at AGS energies as long as the system stays in the hadronic phase. On the other hand, our simulations show that models like Fritiof that do not include rescattering fail to reproduce the pseudorapidity distribution of the transverse energy and particle multiplicity. However, the total transverse energy produced by Fritiof is close to the measured one. This implies that the apparent successes of this model in reproducing experimental $d\sigma/dE_T$ distributions is somewhat fortuitous.

ACKNOWLEDGMENTS

We acknowledge the excellent support of the BNL-AGS and Tandem staff and expert help of Dr. H. Brown and R. Hutter. This work was supported by the U.S. Department of Energy, the National Science Foundation, the Natural Sciences and Engineering Research Council of Canada, and the Conselho National de Pesquisa e Desenvolvimento (CNPq).

[1] E814 Collaboration, J. Barrette *et al.*, Phys. Rev. Lett. **64**, 1219 (1990).
[2] E814 Collaboration, J. Barrette *et al.*, Phys. Rev. C **50**, 3047 (1994).
[3] E802 Collaboration, T. Abbott *et al.*, Phys. Rev. Lett. **64**, 847 (1990).
[4] E814 Collaboration, T.K. Hemmick *et al.*, Nucl. Phys. **A566**, 435c (1994).
[5] E814 Collaboration, J. Barrette *et al.*, Z. Phys. C **59**, 211 (1993).
[6] J. Stachel and G.R. Young, Annu. Rev. Nucl. Part. Sci. **42**, 537 (1992).
[7] E814 Collaboration, J. Stachel *et al.*, Nucl. Phys. **A566**, 183c (1994).
[8] P. Braun-Munzinger, J. Stachel, J.P. Wessels, and N. Xu, Phys. Lett. B **344**, 43 (1995).
[9] E802 Collaboration, T. Abbott *et al.*, Phys. Rev. C **45**, 2933 (1992).
[10] E802 Collaboration, T. Abbott *et al.*, Phys. Rev. D **45**, 3906 (1992).
[11] T. Ludlam, A. Pfoh, and A. Shor, in *Proceedings of the RHIC Workshop 1, Upton, 1985*, edited by P. Haustein and C. Woody (BNL Report No. 51921).
[12] B. Anderson, G. Gustafson, and B. Nilsson-Almqvist, Nucl. Phys. **B281**, 289 (1987).
[13] H. Sorge *et al.*, Nucl. Phys. **A525**, 95c (1991).
[14] Y. Pang, T.J. Schlagel, and S.H. Kahana, Phys. Rev. Lett. **68**, 2743 (1992).
[15] J.D. Bjorken, Phys. Rev. D **27**, 140 (1983).
[16] E814 Collaboration, J. Barrette *et al.*, Phys. Rev. C **46**, 312 (1992).
[17] E814 Collaboration, J. Barrette *et al.*, Phys. Rev. Lett. **70**, 2996 (1993).
[18] E814 Collaboration, J. Barrette *et al.*, Phys. Rev. C **45**, 819 (1992).
[19] J. Simon-Gillo, A. Farooq, M.W. Rawool-Sullivan, A. Ray, J. Shoemaker, J.P. Sullivan, K.L. Wolf, E.F. Barasch, J.G. Boissevain, J.W. Sunier, H. van Hecke, and B. Wolf, Nucl. Instrum. Methods A **309**, 427 (1991).
[20] D. Fox, J. Simon-Gillo, M.W. Rawool-Sullivan, J.G. Boissevain, W.E. Cleland, A. Gavron, B.V. Jacak, D. Kraus, W. Sondheim, J.P. Sullivan, J.W. Sunier, H. van Hecke, S. Watson, and K.L. Wolf, Nucl. Instrum. Methods A **317**, 474 (1992).
[21] M.K. Jayananda, Ph.D. dissertation, University of Pittsburgh, 1991 (unpublished).
[22] R. Brun *et al.*, *GEANT 3 Users Guide*, CERN Data Handling Division, Report No. DD/EE/84-1.
[23] L.S. Waters, Ph.D. dissertation, Stony Brook, 1991 (unpublished).
[24] A. Shor and R. Longacre, Phys. Lett. B **218**, 100 (1989).
[25] J.P. Sullivan, M.W. Rawool-Sullivan, J.G. Boissevain, D. Fox, A. Gavron, K. Holzscheiter, B.V. Jacak, J. Simon-Gillo, W.E. Sondheim, H. van Hecke, B. Wolf, and K.L. Wolf, Nucl. Instrum. Methods A **324**, 441 (1993).
[26] Z. Zhang, P. Braun-Munzinger, W.E. Cleland, G. David, and D. Lissauer, Nucl. Instrum. Methods A **343**, 610 (1994).
[27] Z. Zhang, Ph.D. dissertation, University of Pittsburgh, 1993 (unpublished).
[28] E802 Collaboration, W.A. Zajc *et al.*, Nucl. Phys. **A544**, 237c (1992).
[29] E802 Collaboration, T. Abbott *et al.*, Phys. Rev. Lett. **66**, 1567 (1991).